Article:
Potts, J. and Painter, K.J. (2021) Stable steady-state solutions of some biological aggregation models. SIAM Journal on Applied Mathematics, 81 (3). pp. 1248-1263. ISSN: 0036-1399

https://doi.org/10.1137/20M1348066

STABLE STEADY-STATE SOLUTIONS OF SOME BIOLOGICAL AGGREGATION MODELS*

JONATHAN R. POTTS† AND KEVIN J. PAINTER‡

Abstract. Aggregation phenomena occur across the biological sciences, from cell adhesion to insect swarms, animal home ranges to human cities. Understanding the mechanisms by which they may spontaneously emerge has therefore generated much interest from applied mathematicians. Partial differential equations (PDEs) with non-local advection offer a popular formalism for studying aggregations. However, the inherent non-locality, often necessary for ensuring continuum models are well-posed, makes their study technically challenging. Here, we take a different approach, by studying a discrete-space system that can be formally related to classical non-local PDE approaches via a limiting procedure. We show how to find expressions for the asymptotically-stable steady-states of this discrete-space system, via an energy functional approach. This allows us to predict the size of aggregations as a function of the underlying movement mechanisms of individual organisms. We apply this to a recent model of cell adhesion, revealing a hysteresis property whereby the existing aggregations may persist even as the adhesion tendency decreases past the bifurcation point. We compare this to numerical solutions of the associated non-local PDE system, showing that the hysteresis property predicted by the discrete-space expressions is also present in the continuum system.

Key words. Aggregation equation, bifurcation, cell adhesion, hysteresis, non-local taxis, partial differential equation

AMS subject classifications. 35B32, 35B36, 35B40, 35G20, 35Q92, 92B05

1. Introduction.

Spontaneous aggregations emerge in a wide range of natural systems. For example, individual animals often aggregate into swarms, herds, schools, or flocks [30, 20, 35]; cells can aggregate to form various phenomena, such as muscle tissue, slime mould plasmodia, cancers, and embryos [12, 19, 32]; humans aggregate in cities and towns [36], and many other animal species group themselves into home ranges, each confining their movements to a smaller area than their locomotive capabilities allow [7].

Mathematical models are key to understanding the mechanisms that give rise to such aggregated phenomena. Often they take the form of advection-diffusion equations, with a non-local advection term modelling the movement of individuals in response to the presence of others [24, 23, 33, 18]. Indeed, equations with non-local advection are sometimes termed 'aggregation-diffusion equations' to emphasise the key emergent phenomenon they capture [13]. However, not all the non-local advection-diffusion equations that have been used to model biological aggregations fit neatly into the usual definition of an aggregation-diffusion equation [11].

The popularity of non-local advection-diffusion equations is in part due to their successful usage in answering a broad range of biological questions. For example, [3] used such equations to understand cell sorting behaviours, whereby homogeneous mixtures of two different cell types spontaneously separate into specific arrangements. They showed that this behaviour can be explained by a process of cell-cell adhesion, thus verifying mechanistic hypotheses behind observed spatial patterns. To give an ex-

*Submitted to the editors on 24th June 2020.

†School of Mathematics and Statistics, University of Sheffield, Hicks Building, Hounsfield Road, Sheffield, S3 7RH, UK (j.potts@sheffield.ac.uk, http://jonathan-potts.staff.shef.ac.uk/).

‡Dipartimento Interateneo di Scienze, Progetto e Politiche del Territorio (DIST), Viale Pier Andrea Mattioli, 39, 10125 Torino, Italy. (kevin.painter@polito.it, http://www.macs.hw.ac.uk/~painter/).

ample from animal ecology, [4] showed how locust swarms, consisting of one grouping on the ground and another separate collective in the air, can emerge from long-range (non-local) attraction and short-range repulsion. Non-local advection-diffusion equations were also used by [8] to show how wolves form home ranges, in the absence of conspecifics, from non-local attraction to their own scent markings. Models for human pedestrian flow have also been proposed using a non-local advection-diffusion formalism [16].

Given the broad applicability of non-local advection-diffusion equations, combined with the non-trivial technical aspects of dealing with non-locality, there has been significant mathematical attention paid to such equations in recent years. These include classical questions of existence and uniqueness, pattern formation properties, blow-up, and bifurcations (e.g. [33, 5, 22, 6, 9, 14, 21]). Furthermore, these are often tied to important physical or biological questions. For good recent reviews see [13, 15, 11].

Despite this proliferation of research attention, to our knowledge the question of predicting aggregation size, given the underlying adhesion mechanisms, has not yet been explicitly examined. However, the ability to predict the size of aggregations from the underlying mechanisms is of clear biological importance. If it were possible to find exact expressions for steady-state solutions, an answer to this question would naturally follow, as would other properties such as bifurcation structures and the existence (or otherwise) of hysteresis. However, this is not a trivial task, given the technical difficulties inherent in using non-local advection.

Here, rather than using the formalism of non-local advection-diffusion equations directly, we instead search for steady-state solutions in a one-dimensional discrete-space system of ordinary differential equations (ODEs) that is formally related to a wide class of non-local advection-diffusion equations. Specifically, the continuum limit of our discrete-space system is identical to the local limit of the non-local advection diffusion equations (where the local limit is defined to be the limit as the non-local averaging becomes arbitrarily narrow). The advantage of our approach is that we are able to find an exact formulation of the stable steady-states of the system, via minimising the associated energy (or Lyapunov) functional. This then enables us to calculate exactly the size of any resulting aggregation, as well as revealing bifurcation structures and hysteresis properties.

To demonstrate our technique, we apply it to a specific model of cell-cell adhesion introduced in [25]. This model is a non-local advection-diffusion equation, but we focus first on the associated local discrete-space system. We show how the height and width of resulting aggregations (in discrete-space) depend on the underlying mechanisms: the adhesion rate, the population size, and the 'packing constraint' (ensuring one cannot have an arbitrarily large number of cells at a given point). We also reveal hysteresis in the system, whereby for certain parameters the system has a constant stable steady-state as well as a stable steady-state where aggregations occur. We use the resulting solutions to construct a bifurcation diagram which we verify through numerical bifurcation analysis of the underlying discrete-space system of ODEs.

We then demonstrate, via numerical simulations, that the associated non-local continuum model – the one originally introduced in [25] – also has a similar bifurcation structure. Indeed, as the length scales in the non-local terms are decreased in size (i.e. towards the local limit), the parameter regime where we observe hysteresis appears to tend towards that predicted by the discrete-space solutions. This demonstrates that insights from our discrete-space model can be used to inform properties of the non-local advection-diffusion equation that may be difficult to ascertain by

directly analysing the continuum model. The success of this example suggests that our method may be widely applicable in understanding steady-states of non-local advection-diffusion equations more generally.

The paper is organised as follows. In Section 2 we motivate the problem from the perspective of non-local continuous-space models. Section 3 outlines our approach to examining biological aggregations using discrete-space systems. Section 4 gives detailed analysis of a particular model of cell adhesion in a discrete-space setting. Section 5 compares the results in the discrete-space setting with numerics from the motivating non-local continuous-space model. Section 6 gives some discussion of the results, together with concluding remarks.

2. Motivation from non-local continuous-space models. Our analysis is motivated by two 1D examples of non-local advection-diffusion equations. The first is given as follows

$$\frac{\partial u}{\partial t} = \frac{\partial^2}{\partial x^2}[D(u)] - \frac{\partial}{\partial x}\left[\chi(u)\int_{-\infty}^{\infty}\frac{s}{|s|}\Omega_\xi(|s|)u(x+s,t)\mathrm{d}s\right]. \tag{2.1}$$

Here, $u(x,t)$ is the density of individuals (cells or organisms) at location x and time t; $D(u)$ and $\chi(u)$ are smooth functions. The function $\Omega_\xi(s)$ is defined on $[0,\infty)$ and has a local limit that satisfies

$$\lim_{\xi\to 0}\int_0^\infty s^{2n+1}\Omega_\xi(s)\mathrm{d}s = \begin{cases}\frac{1}{2}, & \text{for } n=0,\\ 0, & \text{for } n\in\mathbb{Z}_{>0}.\end{cases} \tag{2.2}$$

An example of such a function would be $\Omega_\xi(s) = e^{-s/\xi}/(2\xi^2)$. Here, attraction between organisms is greater when they are closer together and gradually decays as the distance between them increases. In this example, interactions extend to an arbitrarily large distance between organisms, albeit with strength that decays exponentially. To circumvent this, functions that are zero for large s, such as $\Omega_\xi(s) = 1/\xi^2$ (resp. $\Omega_\xi(s) = 0$) for $s < \xi$ (resp. $x \geq \xi$), are sometimes used instead. Examples of the model in Equation (2.1) can be found in, e.g. [24, 25].

The second class of non-local advection-diffusion model pertinent to our work is

$$\frac{\partial u}{\partial t} = \frac{\partial^2}{\partial x^2}[D(u)] - \frac{\partial}{\partial x}\left[\chi(u)\frac{\partial}{\partial x}(\mathcal{K}_\xi * u)\right]. \tag{2.3}$$

Here, $\mathcal{K}_\xi(x)$ is a probability density function, defined on $\mathbb{R}$ and symmetric about 0, such that $\lim_{\xi\to 0}\mathcal{K}_\xi(x) = \delta(x)$, the Dirac delta function. For example, one might choose $\mathcal{K}_\xi(x) = e^{-|x|/\xi}/(2\xi)$. Also, $\mathcal{K}_\xi * u$ is the following convolution

$$(\mathcal{K}_\xi * u)(x) = \int_{-\infty}^{\infty}\mathcal{K}_\xi(y-x)u(y)\mathrm{d}y. \tag{2.4}$$

Examples of the model in Equation (2.3) can be found in, e.g. [33, 10, 31].

Equation (2.1) can often be written in the form of Equation (2.3) [11]. This is possible when one can construct a function $\mathcal{K}_\xi(x)$, symmetric about the origin, such that $\mathcal{K}_\xi'(x) = \Omega_\xi(x)$ for $x > 0$, and $\lim_{x\to\pm\infty}\mathcal{K}_\xi(x) = 0$ (details in Appendix A of [11]). However, here we separate Equations (2.1) and (2.3) out, as the two forms each appear in slightly different parts of the literature.

The characteristic width, ξ, of the non-local kernels, Ω_ξ and $\mathcal{K}_\xi$, will clearly have an effect on the size of the aggregation that emerges. Consequently it is valuable to

examine the limit as $\xi \to 0$. For both models (Equations (2.1) and (2.3)), this limit leads to the following equation

$$\frac{\partial u}{\partial t} = \frac{\partial^2}{\partial x^2}[D(u) - \phi(u)], \tag{2.5}$$

where $\phi'(u) = \chi(u)$.

The trouble with analysing Equation (2.5) directly is that it can be unstable to perturbations at arbitrarily high wavenumbers, i.e. the linear pattern formation problem is ill-posed. To see this, let U be the population size and suppose we are working on the interval $[0, L]$. Let $\bar{u} = u - U/L$ and look for solutions of the form $\bar{u} = u_0 \exp(\sigma t + \mathrm{i}\kappa x)$ valid at short times. Then, by neglecting non-linear terms, Equation (2.5) becomes

$$\sigma \bar{u} = \kappa^2[\chi(U/L) - D'(U/L)]\bar{u}. \tag{2.6}$$

Thus, if $\chi(U/L) > D'(U/L)$ then σ is an increasing (quadratic) function of κ, so the linear stability problem is ill-posed: Equation (2.5) is unstable to perturbations at arbitrarily high wavenumbers. Conversely, if $\chi(U/L) \leq D'(U/L)$ then σ is non-positive for all values of κ, so patterns cannot form from small perturbations of the constant steady-state solution.

To circumvent this problem, we instead study a discrete-space model that, being a system of ordinary differential equations, has a unique classical solution for any appropriate initial condition. We will then show that this model has a continuum limit that generalises Equation (2.5).

3. A general discrete-space approach. We define our discrete-space model on a one-dimensional lattice with $N+1$ sites, $i \in \{0, \ldots, N\}$, and lattice spacing l. Let $U_i(t)$ be the number of individuals at site i and time t. The movement of individuals is governed by the following equations

$$\begin{aligned}
\frac{\mathrm{d}U_0}{\mathrm{d}t} &= \lambda[T_d(U_1) - T_d(U_0)], \\
\frac{\mathrm{d}U_i}{\mathrm{d}t} &= \lambda[T_d(U_{i-1}) - 2T_d(U_i) + T_d(U_{i+1})], \qquad \text{for } i \in \{1, \ldots, N-1\}, \\
\frac{\mathrm{d}U_N}{\mathrm{d}t} &= \lambda[T_d(U_{N-1}) - T_d(U_N)],
\end{aligned} \tag{3.1}$$

where $T_d(U_i)$ is a non-constant, analytic function and λ is the jump-rate between adjacent sites. In principle, $T_d(U_i)$ can be arbitrary, but in Section 4 we examine a specific functional form relevant to biological aggregations. Taking the limit as

$$\lambda, N, i \to \infty;\ l \to 0;\ l^2\lambda \to d;\ il \to x;\ lN \to L \tag{3.2}$$

where $d, x, L \in \mathbb{R}_{>0}$ leads to the following partial differential equation (Appendix A)

$$\frac{\partial u}{\partial t} = d\frac{\partial^2}{\partial x^2}[T_c(u)], \tag{3.3}$$

defined on $[0, L]$ with zero-flux boundary conditions, where $u(x,t) = \lim[U_{\lfloor x/l \rfloor}(t)/l]$ is the density of individuals at location x and time t, and $T_c[u(x,t)] = \lim T_d[U_{\lfloor x/l \rfloor}(t)]/l$.

Notice that, if $T_c(u) = [D(u) - \phi(u)]/d$, Equation (3.3) is exactly the same as Equation (2.5). This formalises the relationship between the discrete-space models

studied in this section (System 3.1) and the non-local continuum models discussed in Section 2 (Equations (2.1) and (2.3)), the latter of which are prevalent in the literature [1, 24, 3, 33, 25, 10].

A direct calculation reveals that Equation (3.1) conserves mass, i.e.

$$\frac{\mathrm{d}}{\mathrm{d}t}\sum_{i=0}^{N} U_i = 0, \tag{3.4}$$

so let P_d be the total size of the population. Another direct calculation shows that steady-states of Equation (3.1) occur whenever there is some constant μ such that

$$T_d(U_i) = \mu \tag{3.5}$$

for all $i \in \{0, \ldots, N\}$. An example of this situation is given in Figure 1.

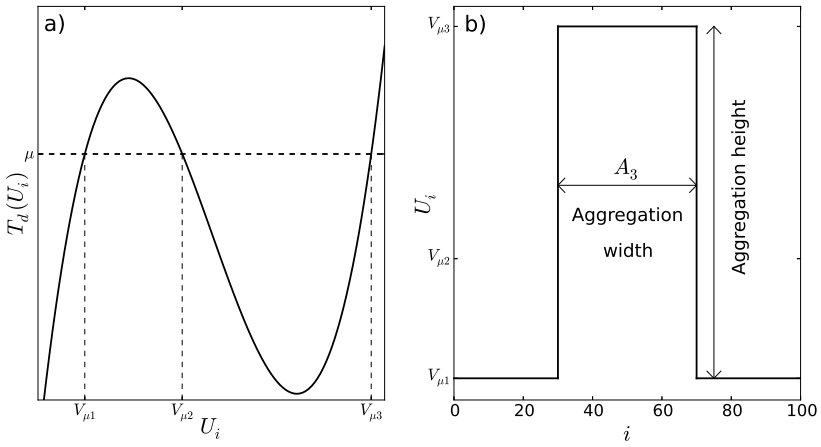

FIG. 1. **Graphical explanation of notation.** *Panel (a) shows an example function for $T_d(U_i)$. Steady-states of System (3.1) occur whenever there is some constant μ such that $T_d(U_i) = \mu$ for all $i \in \{0, \ldots, N\}$ (Equation 3.5). In the example shown, there are three possible values that U_i can take for the particular given value of μ. These are denoted by $V_{\mu 1}, V_{\mu 2}, V_{\mu 3}$. Panel (b) illustrates one possible corresponding steady-state solution. We denote by A_j the number of integers i for which $U_i = V_{\mu j}$ ($j = 1, 2, 3$). In this example, $A_1 = 60, A_2 = 0$, and $A_3 = 41$ (only A_3 is shown on the graph, for simplicity). Note that, by construction, $A_1 + A_2 + A_3 = N + 1$ where $N + 1$ is the number of lattice sites, and $A_1 V_{\mu 1} + A_2 V_{\mu 2} + A_3 V_{\mu 3} = P_d$, where P_d is the total population size (see Equations 3.9 and 3.10). This constrains the set of possible steady-state solutions associated to each μ. Note also that no value of U_i can be greater than P_d (or less than 0) for any i, so values of μ for which the roots of $T_d(U_i) = \mu$ are all greater than P_d (or less than 0) cannot lead to steady-state solutions to System 3.1.*

The first task in understanding the formation of aggregations is to examine when the constant steady-state, $U^* = P_d/(N+1)$, is unstable to linear perturbations (here the superscript asterisk is used to denote steady-state, and recall that P_d is the total population size). In such cases, small spatially non-constant perturbations grow in time and may end up forming aggregations spontaneously. To this end, let $\bar{U}_i = U_i - U^*$ and $\mathbf{W} = (\bar{U}_0, \ldots, \bar{U}_N)^T$. Then, after neglecting non-linear terms, we arrive

at the following matrix equation

$$\frac{\mathrm{d}\mathbf{W}}{\mathrm{d}t} = \lambda T_d'(U^*) A \mathbf{W},$$

$$A = \begin{pmatrix} -1 & 1 & 0 & \dots & 0 & 0 & 0 \\ 1 & -2 & 1 & \dots & 0 & 0 & 0 \\ 0 & 1 & -2 & \dots & 0 & 0 & 0 \\ \vdots & \vdots & \vdots & \ddots & \vdots & \vdots & \vdots \\ 0 & 0 & 0 & \dots & -2 & 1 & 0 \\ 0 & 0 & 0 & \dots & 1 & -2 & 1 \\ 0 & 0 & 0 & \dots & 0 & 1 & -1 \end{pmatrix}. \tag{3.6}$$

It was shown in [2] that the eigenvalues of A all lie in $(-4, 0]$. In particular, they are non-positive, so for the eigenvalues of the matrix $T_d'(U^*)A$ to be positive, we require the value of $T_d'(U^*)$ to be negative. In this case the constant steady state is linearly unstable at all eigenvalues, suggesting that in the $T_d'(U^*) < 0$ region patterns will form spontaneously.

It may also be possible for patterns to form due to the effect of non-linear terms outside the region of linear instability. To determine whether this is the case, we find non-constant stable steady-states of the system by using an energy (or Lyapunov) functional approach. The energy functional for Equation (3.1) has the following form

$$E_d[U_0(t), \dots, U_N(t)] = \sum_{i=0}^{N} F_d(U_i), \tag{3.7}$$

where $F_d'(U_i) = T_d(U_i)$. The following calculation shows that E_d can never increase over time

$$\begin{aligned} \frac{\mathrm{d}E_d}{\mathrm{d}t} &= \sum_{i=0}^{N} \frac{\mathrm{d}U_i}{\mathrm{d}t} T_d(U_i) \\ &= \lambda T_d(U_0)[T_d(U_1) - T_d(U_0)] + \lambda T_d(U_N)[T_d(U_{N-1}) - T_d(U_N)] \\ &\quad + \lambda \sum_{i=1}^{N} [T_d(U_{i-1}) - 2T_d(U_i) + T_d(U_{i+1})] T_d(U_i) \\ &= -\lambda \sum_{i=1}^{N} [T_d(U_i) - T_d(U_{i-1})]^2 \leq 0. \end{aligned} \tag{3.8}$$

Provided Equation (3.7) is bounded below (which we show later), System (3.1) will thus tend towards a local minimum of Equation (3.7). This local minimum occurs when the derivative of E_d is zero, which coincides with the values of U_i where Equation (3.5) is satisfied. Thus, finding the stable steady-states of System (3.1) requires us to find local minima of Equation (3.7) that also satisfy Equation (3.5).

It is possible to find these local minima via a search through a finite range of possibilities, as follows. For each μ (from Equation 3.5), let $\{V_{\mu 1}, \dots, V_{\mu M_\mu}\}$ be the real-valued solutions to Equation (3.5) such that $0 \leq V_{\mu j} \leq P_d$ (see Figure 1). (Here, M_μ is the number of real-valued solutions to Equation (3.5).) Finding the local minima of Equation (3.7), requires searching through all possible μ and

$A_1, \ldots, A_{M_\mu} \in \{0, \ldots, N\}$ such that

$$P_d = \sum_{j=1}^{M_\mu} A_j V_{\mu j}, \tag{3.9}$$

$$N + 1 = \sum_{j=1}^{M_\mu} A_j. \tag{3.10}$$

Since $V_{\mu j}$ must be both non-negative and less than or equal to P_d, for all j, we need only search through $\mu \in [\mu_{\min}, \mu_{\max}]$ where $\mu_{\min} = \min_{U_i}\{T_d(U_i)|0 \le U_i \le P_d\}$ and $\mu_{\max} = \max_{U_i}\{T_d(U_i)|0 \le U_i \le P_d\}$. Thus we have restricted our search for minimum energy solutions to a finite range of values for μ and $A_1, \ldots, A_{M_\mu}$. This both eases the computational requirement for finding minimum energy solutions and shows that the energy functional (Equation 3.7) is bounded, so tends to a local minimum. In the next section, we will demonstrate this search using a specific functional form of $T_d(U_i)$ relevant to contact attraction models of collective cell movement. These are models of cell movement whereby contact between cells causes mutual attraction.

4. Analysis of a discrete-space contact-attraction model. Here, we apply the technique detailed in Section 3 to a specific model of cell aggregations. The model is in the form of Equation (3.1) with

$$T_d(U_i) = U_i - \phi(U_i), \quad \phi(U_i) = \frac{RU_i^2}{6}(3K - 2U_i), \tag{4.1}$$

where $R > 0$ and $K > 0$ are constants. The motivation for studying this particular formalism is that it is related to a model of cell aggregations from a contact-attraction process introduced in [25]. This relationship is detailed in Appendix B.

We begin by stating a criterion for the constant steady-state, $U_i = P_d/(N + 1)$, being unstable to small perturbations. Equation (3.6) and the subsequent text gives the general criterion $T_d'(P_d/(N + 1)) < 0$, which, for our specific choice of T_d, rearranges to give the following

$$\frac{KR - \sqrt{K^2R^2 - 4R}}{2R} < \frac{P_d}{N+1} < \frac{KR + \sqrt{K^2R^2 - 4R}}{2R} \quad \text{and} \quad K^2R > 4. \tag{4.2}$$

Next, we use the energy method from Section 3 to search for the global steady-state solution to Equations (3.1) and (4.1). Although this method can be used to find any local minimum, we restrict our search to the global minimum, for simplicity. In Equation (4.1), $T_d(U_i)$ is a cubic. Therefore, for each $\mu \in \mathbb{R}$, there are at most three real-valued solutions to $T_d(U_i) = \mu$ for $\mu \in [\mu_{\min}, \mu_{\max}]$ and at least one. Let $V_{\mu 1}, V_{\mu 2}, V_{\mu 3}$ denote these three solutions, if all three exist (so that $T_d(V_{\mu 1}) = T_d(V_{\mu 2}) = T_d(V_{\mu 3}) = \mu$). If there are only two distinct real-valued solutions, denote them by $V_{\mu 1}, V_{\mu 2}$ and set $V_{\mu 3} = V_{\mu 2}$. If there is only one real-valued solution, denote it by $V_{\mu 1}$ and set $V_{\mu 3} = V_{\mu 2} = V_{\mu 1}$. Denote by $A_1 \in \{0, \ldots N\}$ (resp. A_2, A_3) the number of sites that contain $V_{\mu 1}$ (resp. $V_{\mu 2}, V_{\mu 3}$) individuals, setting $A_3 = 0$ if $V_{\mu 3} = V_{\mu 2}$ and $A_2 = 0$ if $V_{\mu 2} = V_{\mu 1}$.

If there are only two real-valued solutions to $T_d(U_i) = \mu$ then, by Equation (3.10), $A_2 = N+1-A_1$. If there are three real-valued solutions then, by Equations (3.9-3.10),

we have

$$A_2 = \frac{P_d + A_2(V_{\mu 3} - V_{\mu 1}) - V_{\mu 3}(N+1)}{V_{\mu 2} - V_{\mu 3}}, \tag{4.3}$$

$$A_3 = N + 1 - A_2 - A_1. \tag{4.4}$$

Consequently, to find the minimum energy solutions, we need only search through values of $\mu \in [\mu_{\min}, \mu_{\max}]$ and $A_1 \in \{0, \dots, N\}$. Then A_2 and A_3 are determined by Equations (4.3) and (4.4) respectively, whilst $V_{\mu 1}, V_{\mu 2}, V_{\mu 3}$ are given by Equation (3.5).

Due to the constraints on A_1, A_2, A_3 (Equation 4.3, 4.4) and the fact that they all have to be elements of $\{0, \dots, N\}$, the magnitude of N may have an effect on the existence of a non-constant minimum-energy solution. In reality, organisms will be able to move continuously in space, not being constrained by a lattice. Therefore it is valuable to search for minimum energy solutions in the large-N limit. Specifically, we take the limit given in (3.2), additionally with $\mu \to 0$ such that $\mu/l \to m$ with $0 < m < \infty$. This latter limit is required to find a solution to $T_c[u(x,t)] = m$ that corresponds to the continuum limit of $T_d(U_i) = \mu$, where $T_c[u(x,t)] = \lim[T_d(U_i)/l]$ (Appendix A).

In this limit, $T_c(u) = u - ru^2(3k - 2u)/6$ and $x \in [0, L]$ (Appendix B, Equation (B.2)). To reduce parameters, we non-dimensionalise, using the following substitutions

$$\begin{gathered} \tilde{x} = \frac{x}{L}, \, \tilde{t} = \frac{tD}{L^2}, \, \tilde{u}(\tilde{x}, \tilde{t}) = \frac{u(x,t)}{k}, \, \tilde{r} = rk^2, \\ \tilde{a}_j = \frac{a_j}{L}, \, \tilde{T}_c(\tilde{u}) = \frac{T_c(u)}{k}, \, P = \frac{P_d L}{k}, \, \tilde{m} = \frac{m}{k}. \end{gathered} \tag{4.5}$$

We henceforth drop the tildes for notational convenience. Then suppose there are three distinct, real solutions to $T_c(u) = m$ and denote them by v_{m1}, v_{m2}, v_{m3}. We arrive at the following expressions

$$T_c(u) = u - \frac{ru^2}{6}(3 - 2u), \tag{4.6}$$

$$a_2 = \frac{P + a_1(v_{m3} - v_{m1}) - v_{m3}}{v_{m2} - v_{m3}}, \tag{4.7}$$

$$a_3 = 1 - a_1 - a_2, \tag{4.8}$$

$$\mathcal{E}_c(m, a_1) = \sum_{j=1}^{3} a_j \left[\frac{v_{mj}^2}{2} - \frac{r v_{mj}^3}{6} + \frac{r v_{mj}^4}{12} \right]. \tag{4.9}$$

Here, $\mathcal{E}_c(m, a_1)$ is the energy, expressed as a function of m and a_1. If there are only two distinct real-valued solutions to $T_c(u) = m$ then denote them by v_{m1} and v_{m2}; then set $v_{m3} = v_{m2}$, $a_2 = 1 - a_1$, and $a_3 = 0$. If there is only one distinct real-valued solution to $T_c(u) = m$ then denote it by v_{m1}; then set $v_{m3} = v_{m2} = v_{m1}$, $a_1 = 1$, $a_2 = 0$, and $a_3 = 0$. Finding the global steady-state solution requires finding the minimum of $\mathcal{E}_c(m, a_1)$ across all values of $m \in [m_{\min}, m_{\max}]$ and $a_1 \in [0, 1]$ such that $a_2, a_3 \in [0, 1]$ and $v_{m1}, v_{m2}, v_{m3} \geq 0$, where $m_{\min} = \min_u\{T_c(u) | 0 \leq u \leq P\}$ and $m_{\max} = \max_u\{T_c(u) | 0 \leq u \leq P\}$.

The resulting large-N limit of the global minimum energy solution to Equation

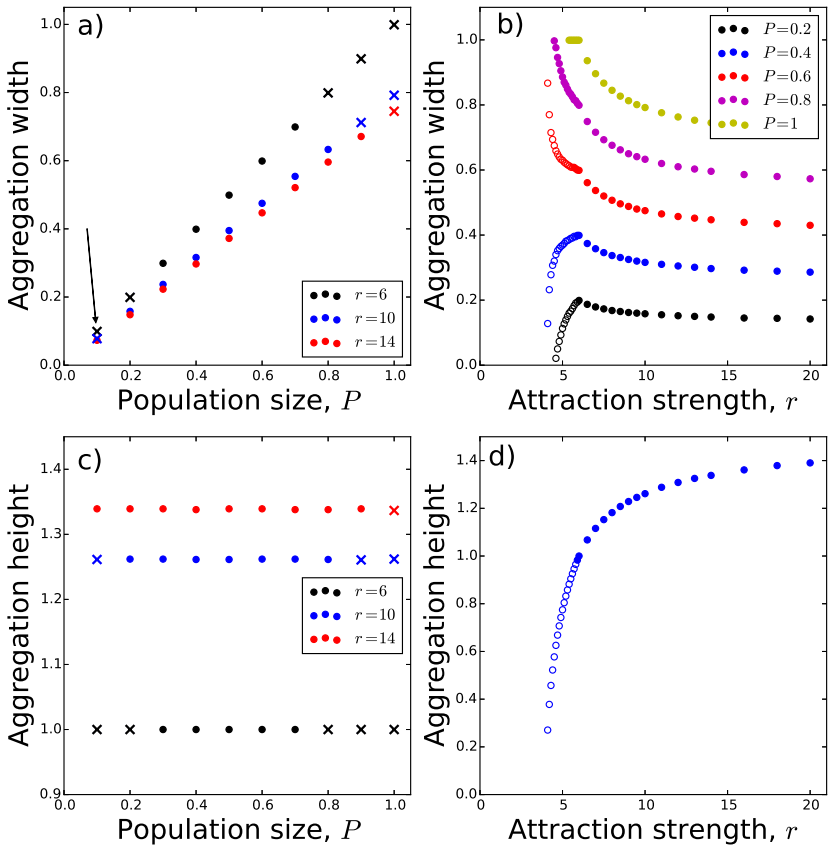

FIG. 2. **Predicted aggregation width.** *Panel (a) shows the effect of the population size, P, on the aggregation width. Dots (resp. crosses) denote situations where the constant steady-state is unstable (resp. stable) to linear perturbations. Note that, in some cases (e.g. $P = 0.1, r = 6$, see arrow in Panel a), the constant steady-state is stable, yet the global minimum energy solution is an aggregation. This indicates a hysteresis in the system, whereby aggregations will remain if already formed, but not arise spontaneously from small perturbations of the spatially constant solution. In Panel (b), we see how the aggregation width varies with the strength of contact attraction, r. The solid dots denote 'pure' aggregations whereby only one of $v_{m_*1}, v_{m_*2}, v_{m_*3}$ (defined in Equation 4.10) is greater than zero. The unfilled circles represent situations whereby more than one of $v_{m_*1}, v_{m_*2}, v_{m_*3}$ is greater than zero. Panels (c) shows that P appears not to affect the aggregation height (defined as $\max_j\{v_{m_*j}\} - \min_j\{v_{m_*j}\}$). Panel (d) shows the effect of r on aggregation height.*

255 (3.1), which we denote by $u_*(x)$, has the following functional form

$$u_*(x) = \begin{cases} v_{m_*1}, & \text{on a subset } S_1 \subseteq [0,1] \text{ of measure } a_1, \\ v_{m_*2}, & \text{on a subset } S_2 \subseteq [0,1] \text{ of measure } a_2, \\ v_{m_*3}, & \text{on a subset } S_3 \subseteq [0,1] \text{ of measure } a_3, \end{cases} \tag{4.10}$$

256 for some m_*, using the definitions of v_{mj} and a_j ($i \in \{1,2,3\}$) from the previous

paragraph. Here, S_1, S_2, S_3 are pairwise disjoint and $u_*(x)$ is the continuum limit of the minimum energy solution for the discrete system (Equation 3.1), with $T_d(U_i)$ as defined in Equation (4.1).

To understand the properties of $u_*(x)$, we calculate it for a range of parameter values, r and P. Without loss of generality, suppose that $v_{m_*1} \geq v_{m_*2} \geq v_{m_*3}$. Then we define a_1 as the *aggregation width* and $v_{m_*1} - v_{m_*3}$ as the *aggregation height* (see Figure 1). (Note that our terminology in calling a_1 the 'aggregation width' is merely a heuristic nomenclature, based on the case where the set S_1 is connected. However, there is no *a priori* reason that S_1 must be connected.)

Figure 2 shows the aggregation width and height for the global minimum energy solution for various values of r and P. For sufficiently large r, it turns out that v_{m_*2} and v_{m_*3} are (numerically) equal to zero. We call this case a *pure aggregation*. These occur for $r \gtrsim 6$ when $P = 0.2, 0.4, 0.6$ and for all values of r we examined when $P = 0.8, 1$. For situations where more than one of v_{m_*1}, v_{m_*2}, v_{m_*3} are greater than zero, it is possible for the whole terrain to have non-zero population density, but have some regions of space where the population density is higher than others.

It is interesting to examine the parameter values for which the constant steady-state is unstable to linear perturbations, and compare this to the set of values where the minimum energy solution is non-constant. The large-N limit, dimensionless version of the instability criterion in Equation (4.2) is that $r > 4$ and $1 - \sqrt{1 - 4/r} < 2P < 1 + \sqrt{1 - 4/r}$. For some parameter values, the constant steady-state is stable, yet the global minimum energy solution is one where there is an aggregation of length less than 1 (see Figure 2a). This indicates a hysteresis in the system, whereby aggregations will persist if present, but will not form spontaneously from a small non-constant perturbation of the constant steady-state.

To understand this hysteresis better, we construct a bifurcation diagram (Figure 3) for the case $P = 0.1$. The top branch gives the aggregation height constructed from the minimum energy solutions. The bottom branch corresponds to the results of linear stability analysis. We then tested the predictions from Equation (4.10) against numerical solutions of the discrete-space system (Equation 3.1) by performing a numerical bifurcation analysis, following the method from [27].

This numerical method begins by setting a start value for the parameter of interest, which in our case is $r = 12$, and solving to numerical steady-state. Then we decrease the value of r, perturb the solution with small random fluctuations, and solve again to numerical steady-state. The process of reducing r, perturbing the solution, and solving to steady-state is then repeated until we reach values of r for which the aggregation patterns disappear (see [27] for more details). Figure 3 shows that our predictions are in good agreement with the numerical bifurcation analysis, only slightly over-estimating the bifurcation point ($r = 5.0$ in our predictions and $r \approx 4.8$ for the numerics).

To solve Equation (3.1) numerically, we used a finite difference approximation with time-step $\Delta t = 0.001$ and $N = 100$. We defined the point at which numerical steady-state is reached to be the first point in time where $\sum_i |U_i(t + \Delta t) - U_i(t)| < 10^{-8}$.

5. Numerical comparison with a non-local continuous-space formulation. We explore whether the discrete model predicts behaviour of the associated non-local PDE (Equation 2.1) using numerical bifurcation analysis. The numerical method for solving Equation (2.1) is described in detail in [17], where we set $D(u) = d$,

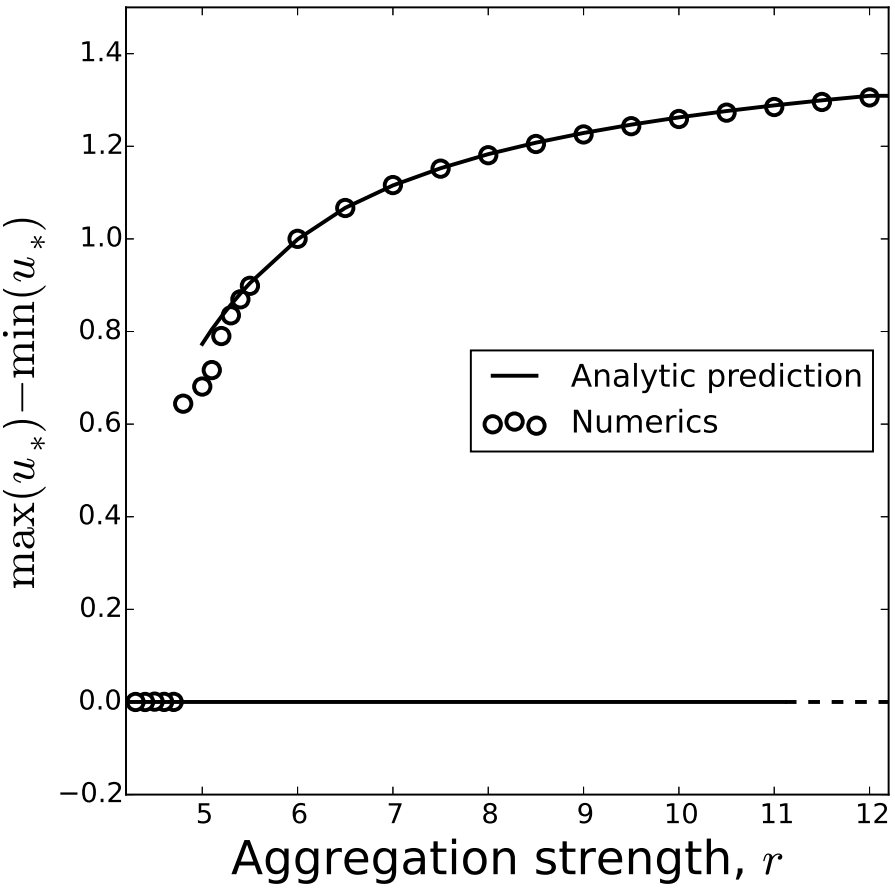

FIG. 3. **Bifurcation diagram.** *The solid and dashed lines give predictions from our analysis regarding the steady-states and their stability. Specifically, the top branch is the global minimum energy solution (see Equation (4.10)), where this corresponds to a non-constant solution. The bottom branch gives the stability of the constant steady-state solution: solid if it is stable and dashed if it is unstable. The circles give numerical steady-state solutions from the numerical bifurcation analysis described in the Main Text. Here,* $P = 0.1$.

$\chi(u) = ru(k-u)$, and the step-form

$$\Omega_\xi(s) = \begin{cases} 1/\xi^2 & s < \xi\,, \\ 0 & \text{otherwise}\,. \end{cases}$$

These choices lead to (B.3) as $\xi \to 0$, which is the continuum limit of the discrete-space model studied in Section 4. As in the discrete model we apply numerical continuation, fixing $P = 0.1$, $k = d = 1$ and treating r as the bifurcation parameter. Bifurcation curves are constructed for various ξ. Note that decreasing ξ increases computational time due to the finer resolution required for the non-local term, reinforcing the need for alternative approaches that do not require numerical solutions, such as those

presented here.

The uniform steady-state of the non-local aggregation model becomes unstable at a critical threshold $r^*(\xi)$: this point is straightforward to determine via linear stability analysis (see [25]) and, for a finite domain, varies a small amount with ξ. As would be expected, as $\xi \to 0$ this converges to the critical value resulting from Equation (2.6).

Upper curves in Figure 4(a) describe solution branches corresponding to a (numerically) stable single aggregate, with specific solutions illustrated in (b) and (c). Each curve is composed from supercritical and subcritical branches that extend about $r^*(\xi)$. Subcritical extensions indicate a corresponding hysteresis phenomenon to that noted for the discrete model. These branches terminate at a lower threshold $r^{**}(\xi)$, below which the aggregating component is overwhelmed by diffusion. Notably, lowering ξ decreases $r^{**}(\xi)$, yet each computed value of $r^{**}(\xi)$ is strictly higher than the corresponding bifurcation point ($r = 5.0$) predicted by our analysis of the discrete-space system (Figure 3). We conjecture that, were it possible to continue the numerical analysis of the non-local continuum model to arbitrarily low values of ξ, the location of $r^{**}(\xi)$ would tend towards $r = 5.0$. Unfortunately, moving $\xi > 0$ considerably below 0.01 becomes computationally infeasible inside a reasonable time frame.

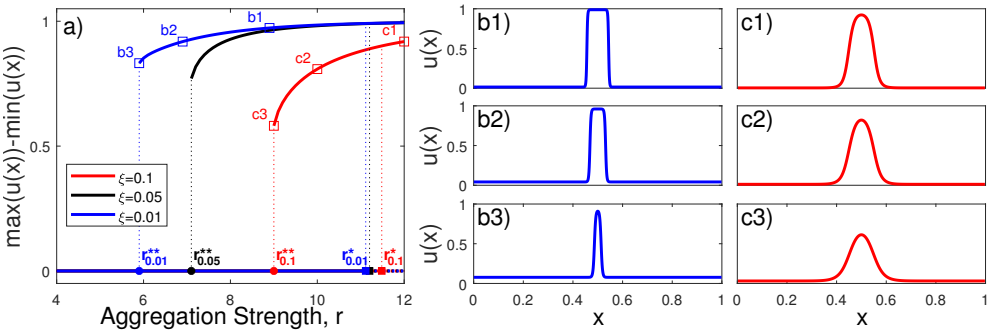

FIG. 4. **Bifurcation diagram for a nonlocal aggregation model.** *(a) Solid lines show (numerically) computed stable steady-states under different values of sensing radius ξ. Specifically, the top branch describes a single cluster with the bottom branch showing the stability of the constant steady-state solution. The bottom branch becomes unstable at the critical threshold r^*_ξ, as predicted via linear stability analysis. The subcritical branch of the single cluster solution remains stable down to some lower threshold r^{**}_ξ, below which the cluster collapses and disperses. Solutions at the points marked by squares are shown in the plots in (b1)-(b3) and (c1)-(c3). For these plots, we set $P = 0.1$, $d = 1$ and $k = 1$.*

6. Discussion. We have shown how to gain understanding into the size and hysteresis properties of biological aggregations by using a discrete-space model. This model can be formally related to the oft-used aggregation equation formalism, but has the advantage of being amenable to exact analysis of the steady-state solutions. We tested our resulting equations against a particular model of cell adhesion and showed that they are in good agreement with discrete-space numerics (Figure 3). Thus this approach provides a quick way of giving quite a detailed description of bifurcation structure in discrete-space aggregation models.

We also investigated the extent to which these predictions carry over to a corresponding non-local continuum model that is often used to study aggregation phenomena (Equation 2.1). This involved numerical simulations of this non-local continuum model, which are summarised in Figure 4. We observe some clear similarities between

the discrete-space results and the continuum results, but also some clear differences.

Notably, guided by the identification of hysteresis in the discrete model, numerical investigation was performed on the continuum model and indeed the same phenomenon was found. Furthermore, as the non-local parameter ξ tends towards zero, the point where the subcritical structure collapses (r_ξ^{**} in Figure 4), appears to tend towards the corresponding point in the discrete-space case (Figure 3). However, numerics for small ξ become increasing time-consuming, so it is of considerable value to have a quick technique for deriving the expected limit of r_ξ^{**} as $\xi \to 0$.

On the other hand, perhaps the biggest discrepancy between the steady-states of the non-local PDE and those of the corresponding discrete-space system is in the height of the resulting aggregation. We see in Figure 4 that the steady-state solution in the continuous case always appears to be bounded by $u = 0$ and $u = 1$. We expect that this arises from the fact that $\chi(u) = ru(k - u)$ vanishes at $u = 0$ and $u = 1$ when $k = 1$. However, the discrete-space system, given by Equations (3.1) and (4.1) for $K = 1$, does give rise to aggregations whose height is greater than 1 (Figure 3). We conjecture that this is because the discrete-space system vanishes at $U_i = 0$ and $U_i = 3/2$ but not when $U_i = 1$. Note that none of the aggregations in the numerical solutions we examined have height greater than $3/2$ (Figure 3). By extension, this means there is also a discrepancy in the aggregation width between the discrete and continuous models.

The discrete-space model studied here only incorporates the effect of nearest-neighbour lattice sites. However, it may be possible to extend our techniques to certain cases where each lattice site is affected by sites beyond its nearest neighbour. Such an extension would lead to a more general form of the matrix A in Equation (3.6). If this new matrix has eigenvalues with negative real parts then the same condition for linear pattern formation would hold as in our work: $T_d'(U^*) < 0$. The next step, which we expect would be non-trivial in general, would be to determine which forms of the matrix A allow for a decreasing energy functional, to give a similar argument to Equation (3.8). This would be an interesting avenue for future work.

Although many recent models of biological aggregation use a non-local continuum model, discrete-space formalisms are not without precedent. Indeed, until [3], it was typical to use a discrete-space formalism to model the specific process of aggregation via cell adhesion (see [3] for references). Perhaps the closest model to the one presented here is that of [2]. There, the authors analyse a specific discrete-space model for linear pattern formation properties and steady-states, but do not examine the stability of non-constant steady-states. Likewise, the effect of the functional form of (3.5) on steady-state patterns was analysed in [34], but without any stability analysis of non-constant steady-states. Here, we build on both studies by providing an energy method to categorise the asymptotic stability of such non-constant steady-states. This makes use of a construction of discrete-space energy functionals from [28]. Our method is framed in a general context (Section 3) that encompasses both the model in [2] and the specific model studied here (Section 4).

PDE formalisms are often used because they are amenable to large swathes of analytic techniques, whereas discrete models often rely on simulation analysis [29]. In contrast, here we given an example of a discrete-space approach that is amenable to analysis that has not so far been possible with continuum descriptions. The difficulty with the continuum approach is the necessity for non-local advection to ensure the problem is well-posed. This disappears in the discrete-space description (indeed, the lattice size can be thought of as analogous to non-locality). By then showing that the steady-states of the discrete system live in a finite set (something that would lead to

trivial solutions in the continuum limit), it is possible to search through the possible steady-state solutions for the minimum energy. This would not be so easy using an energy description of the non-local continuum model, as the search would be through an entire function space rather than a finite set of possible values. In conclusion, we suggest that mathematical analysis of discrete-space approximations should remain a valuable part of the toolkit for anyone studying mathematical models of biological aggregations.

Appendix A. Continuum limit of the general model. Here we show how Equation (3.1) leads to Equation (3.3) in the limit as $\lambda, N, i \to \infty$ and $l \to 0$ such that $l^2\lambda \to d$, $il \to x$, and $lN \to L$ for $d, L \in \mathbb{R}_{>0}$. Using lim to denote this limit, we define $u(x,t) = \lim[U_{\lfloor x/l \rfloor}(t)/l]$ and $T_c[u(x,t)] = \lim T_d[U_{\lfloor x/l \rfloor}(t)]/l$. Then, for $0 < i < N$, we have

$$\lim\left(\frac{1}{l}\frac{\mathrm{d}U_i}{\mathrm{d}t}\right) = \lim\left(\frac{\mathrm{d}}{\mathrm{d}t}\left(\frac{U_{x/l}}{l}\right)\right) = \frac{\partial u}{\partial t}, \tag{A.1}$$

and

$$\begin{aligned}
&\lim\left(\frac{\lambda}{l}[T_d(U_{i-1}) - 2T_d(U_i) + T_d(U_{i+1})]\right)\\
&= \lim\left(\lambda\frac{[T_d(U_{(x-l)/l}) - 2T_d(U_{x/l}) + T_d(U_{(x+l)/l})]}{l}\right)\\
&= \lim\left(\lambda l^2\frac{[T_d(U_{(x-l)/l})/l - 2T_d(U_{x/l})/l + T_d(U_{(x+l)/l})/l]}{l^2}\right)\\
&= d\frac{\partial^2}{\partial x^2}[T_c(u)]. \qquad \text{(A.2)}
\end{aligned}$$

By Equation (3.1), we can equate Equations (A.1) and (A.2) to give

$$\frac{\partial u}{\partial t} = d\frac{\partial^2}{\partial x^2}[T_c(u)], \tag{A.3}$$

which is Equation (3.3).

For the boundary conditions, we can take the continuum limit of either the top or bottom row of Equation (3.1). We start by looking at the bottom row, which gives the zero-flux boundary condition at $x = L$. For the left-hand side, we have

$$\lim\left(\frac{\mathrm{d}U_N}{\mathrm{d}t}\right) = \lim\left(l\frac{\mathrm{d}}{\mathrm{d}t}\left(\frac{U_{L/l}}{l}\right)\right) = 0 \times \left.\frac{\partial u}{\partial t}\right|_{x=L} = 0. \tag{A.4}$$

For the right-hand side (of the bottom row of Equation (3.1)), we have

$$\begin{aligned}
&\lim(\lambda[T_d(U_{N-1}) - T_d(U_N)])\\
&= \lim\left(\lambda l^2\frac{T_d(U_{(L-l)/l})/l - T_d(U_{L/l})/l}{l}\right) = -d\left.\frac{\partial u}{\partial x}\right|_{x=L}. \qquad \text{(A.5)}
\end{aligned}$$

Then Equations (A.4) and (A.5) together give the zero flux boundary condition at $x = L$. The calculation of the boundary condition at $x = 0$ is similar.

Appendix B. Continuum limit of the model in Section 4. Using the notation and limiting procedure from Appendix A, we derive here the continuum

limit of Equation (3.1) in the case where

$$T_d(U_i) = U_i - \frac{RU_i^2}{6}(3K - 2U_i), \tag{B.1}$$

as defined in Equation (4.1). In addition to the limit from Appendix A, we take the limit as $K \to 0$ and $R \to \infty$ such that $K/l \to k$ and $Rl^2 \to r/d$. Then

$$\begin{aligned} dT_c[u(x,t)] &= \lim[l^2 \lambda T_d(U_i)/l] \\ &= \lim\left[\frac{l^2\lambda U_i}{l} - \frac{l^4 \lambda R}{6}\frac{U_i^2}{l^2}\left(\frac{3K}{l} - \frac{2U_i}{l}\right)\right] \\ &= du(x,t) - \frac{ru^2(x,t)}{6}(3k - 2u(x,t)). \end{aligned} \tag{B.2}$$

Hence, by plugging Equation (B.2) into Equation (A.3), the continuum limit of Equation (3.1) with T_d as defined in Equation (4.1) is

$$\begin{aligned} \frac{\partial u}{\partial t} &= d\frac{\partial^2 u}{\partial x^2} - \frac{\partial^2}{\partial x^2}\left[\frac{ru^2}{6}(3k - 2u)\right] \\ &= d\frac{\partial^2 u}{\partial x^2} - \frac{\partial}{\partial x}\left[ru(k-u)\frac{\partial u}{\partial x}\right], \end{aligned} \tag{B.3}$$

which is the local limit (i.e. $\xi \to 0$) of Equation (2.1) with $\chi(u) = ru(k-u)$ and $D(u) = d$. This functional form for $\chi(u)$ was studied by [25]. It incorporates a 'packing' constant, k, accounting for the fact that there is a limit to the amount of individuals that can be in a given area. Specifically, individuals at x at time t will tend to move up (resp. down) the density gradient when $0 < u(x,t) < k$ (resp. $k < u(x,t)$). This feature has been shown to be both mathematically important and biologically realistic in a variety of contexts [26].

Acknowledgements. This research arose from conversations at the workshop 'PDEs in Mathematical Biology: Modelling and Analysis' at the International Centre for Mathematics Sciences, Edinburgh, funded by the London Mathematics Society and Clay Mathematics Institute. We thank all those involved in funding and organising this workshop. We also thank Thomas Hillen and two anonymous reviewers for helpful comments on the manuscript.

REFERENCES

[1] W. Alt, *Degenerate diffusion equations with drift functionals modelling aggregation*, Nonlinear Analysis: Theory, Methods & Applications, 9 (1985), pp. 811–836.
[2] K. Anguige and C. Schmeiser, *A one-dimensional model of cell diffusion and aggregation, incorporating volume filling and cell-to-cell adhesion*, Journal of Mathematical Biology, 58 (2009), p. 395.
[3] N. J. Armstrong, K. J. Painter, and J. A. Sherratt, *A continuum approach to modelling cell–cell adhesion*, Journal of Theoretical Biology, 243 (2006), pp. 98–113.
[4] A. J. Bernoff and C. M. Topaz, *A primer of swarm equilibria*, SIAM Journal on Applied Dynamical Systems, 10 (2011), pp. 212–250.
[5] A. L. Bertozzi and T. Laurent, *Finite-time blow-up of solutions of an aggregation equation in R^n*, Communications in Mathematical Physics, 274 (2007), pp. 717–735.
[6] A. L. Bertozzi and D. Slepcev, *Existence and uniqueness of solutions to an aggregation equation with degenerate diffusion*, Communications on Pure and Applied Analysis, 9 (2009), p. 1617.

[7] L. Börger, B. D. Dalziel, and J. M. Fryxell, *Are there general mechanisms of animal home range behaviour? a review and prospects for future research*, Ecology Letters, 11 (2008), pp. 637–650.
[8] B. Briscoe, M. Lewis, and S. Parrish, *Home range formation in wolves due to scent marking*, Bull. Math. Biol., 64 (2002), pp. 261–284, https://doi.org/10.1006/bulm.2001.0273.
[9] P.-L. Buono and R. Eftimie, *Codimension-two bifurcations in animal aggregation models with symmetry*, SIAM Journal on Applied Dynamical Systems, 13 (2014), pp. 1542–1582.
[10] M. Burger, M. D. Francesco, S. Fagioli, and A. Stevens, *Sorting phenomena in a mathematical model for two mutually attracting/repelling species*, SIAM Journal on Mathematical Analysis, 50 (2018), pp. 3210–3250.
[11] A. Buttenschön and T. Hillen, *Non-local cell adhesion models: Steady states and bifurcations*, arXiv preprint arXiv:2001.00286, (2020).
[12] M. Cabel, H. J. Meiselman, A. S. Popel, and P. C. Johnson, *Contribution of red blood cell aggregation to venous vascular resistance in skeletal muscle*, American Journal of Physiology-Heart and Circulatory Physiology, 272 (1997), pp. H1020–H1032.
[13] J. A. Carrillo, K. Craig, and Y. Yao, *Aggregation-diffusion equations: dynamics, asymptotics, and singular limits*, in Active Particles, Volume 2, Springer, 2019, pp. 65–108.
[14] J. A. Carrillo, F. James, F. Lagoutière, and N. Vauchelet, *The filippov characteristic flow for the aggregation equation with mildly singular potentials*, Journal of Differential Equations, 260 (2016), pp. 304–338.
[15] L. Chen, K. J. Painter, C. Surulescu, and A. Zhigun, *Mathematical models for cell migration: a nonlocal perspective*, Philosophical Transactions of the Royal Society of London B, To appear (2020).
[16] R. M. Colombo, M. Garavello, and M. Lécureux-Mercier, *A class of nonlocal models for pedestrian traffic*, Mathematical Models and Methods in Applied Sciences, 22 (2012), p. 1150023.
[17] A. Gerisch, *On the approximation and efficient evaluation of integral terms in pde models of cell adhesion*, IMA Journal of Numerical Analysis, 30 (2010), pp. 173–194.
[18] A. Gerisch and M. A. Chaplain, *Mathematical modelling of cancer cell invasion of tissue: local and non-local models and the effect of adhesion*, Journal of Theoretical Biology, 250 (2008), pp. 684–704.
[19] V. V. Glinsky, G. V. Glinsky, O. V. Glinskii, V. H. Huxley, J. R. Turk, V. V. Mossine, S. L. Deutscher, K. J. Pienta, and T. P. Quinn, *Intravascular metastatic cancer cell homotypic aggregation at the sites of primary attachment to the endothelium*, Cancer Research, 63 (2003), pp. 3805–3811.
[20] R. Jeanson, C. Rivault, J.-L. Deneubourg, S. Blanco, R. Fournier, C. Jost, and G. Theraulaz, *Self-organized aggregation in cockroaches*, Animal Behaviour, 69 (2005), pp. 169–180.
[21] G. Kaib, *Stationary states of an aggregation equation with degenerate diffusion and bounded attractive potential*, SIAM Journal on Mathematical Analysis, 49 (2017), pp. 272–296.
[22] T. Laurent, *Local and global existence for an aggregation equation*, Communications in Partial Differential Equations, 32 (2007), pp. 1941–1964.
[23] C. T. Lee, M. F. Hoopes, J. Diehl, W. Gilliland, G. Huxel, E. V. Leaver, K. McCann, J. Umbanhowar, and A. Mogilner, *Non-local concepts and models in biology*, Journal of Theoretical Biology, 210 (2001), pp. 201–219.
[24] A. Mogilner and L. Edelstein-Keshet, *A non-local model for a swarm*, Journal of Mathematical Biology, 38 (1999), pp. 534–570.
[25] K. Painter, J. Bloomfield, J. Sherratt, and A. Gerisch, *A nonlocal model for contact attraction and repulsion in heterogeneous cell populations*, Bulletin of Mathematical Biology, 77 (2015), pp. 1132–1165.
[26] K. J. Painter and T. Hillen, *Volume-filling and quorum-sensing in models for chemosensitive movement*, Can. Appl. Math. Quart, 10 (2002), pp. 501–543.
[27] K. J. Painter and T. Hillen, *Spatio-temporal chaos in a chemotaxis model*, Physica D, 240 (2011), pp. 363–375.
[28] K. J. Painter, D. Horstmann, and H. G. Othmer, *Localization in lattice and continuum models of reinforced random walks*, Applied Mathematics Letters, 16 (2003), pp. 375–381.
[29] E. Palsson and H. G. Othmer, *A model for individual and collective cell movement in dictyostelium discoideum*, Proceedings of the National Academy of Sciences, 97 (2000), pp. 10448–10453.
[30] J. K. Parrish and W. M. Hamner, *Animal groups in three dimensions: how species aggregate*, Cambridge University Press, 1997.
[31] J. R. Potts and M. A. Lewis, *Spatial memory and taxis-driven pattern formation in model*

ecosystems, Bulletin of Mathematical Biology, 81 (2019), pp. 2725–2747, https://doi.org/10.1007/s11538-019-00626-9, https://doi.org/10.1007/s11538-019-00626-9.

[32] C. R. Reid and T. Latty, *Collective behaviour and swarm intelligence in slime moulds*, FEMS Microbiology Reviews, 40 (2016), pp. 798–806.

[33] C. M. Topaz, A. L. Bertozzi, and M. A. Lewis, *A nonlocal continuum model for biological aggregation*, Bulletin of Mathematical Biology, 68 (2006), p. 1601.

[34] P. Turchin, *Population consequences of aggregative movement*, Journal of Animal Ecology, (1989), pp. 75–100.

[35] P. A. Westley, A. M. Berdahl, C. J. Torney, and D. Biro, *Collective movement in ecology: from emerging technologies to conservation and management*, Phil. Trans. R. Soc. B, 373 (2018), p. 20170004.

[36] J. Yuan, Y. Zheng, and X. Xie, *Discovering regions of different functions in a city using human mobility and pois*, in Proceedings of the 18th ACM SIGKDD international conference on Knowledge discovery and data mining, 2012, pp. 186–194.